A DECOMPOSITION METHODOLOGY FOR QUANTITATIVE INTERPRETATION OF REACTIVITY EFFECT DISCREPANCIES IN LWR-PROTEUS

R. van Geemert, F. Jatuff, R. Chawla*
Paul Scherrer Institute, Nuclear Energy and Safety Research Department
CH-5232 Villigen PSI, Switzerland
rene.vangeemert@psi.ch, fabian.jatuff@psi.ch, rakesh.chawla@epfl.ch

*Co-affiliation :
Swiss Federal Institute of Technology (EPFL),
CH-1015 Lausanne, Switzerland

ABSTRACT

With reactivity being the most important integral reactor physics quantity – and simultaneously the one that can be measured with the highest accuracy – there is a great interest in understanding how possible space and energy-dependent data and/or modelling discrepancies may propagate into a calculated reactivity change, and with which magnitude this occurs. In the context of pin removal reactivity effects in an LWR assembly, for example, it is illustrative to carry out, for any arbitrary localised material composition perturbation, a *decomposition* of the total effect into individual space and energy-dependent contributions of the different unit cells in the assembly. If this decomposition is normalized to +100 % in the case of a positive reactivity effect, and to -100 % in the case of a negative reactivity effect, an importance map is established that indicates the relative contribution (in percent) of each individual contributing cell to the total reactivity effect caused by the localised material composition change. Such an importance map can be interpreted as a sensitivity matrix that quantifies the final discrepancy in a calculated reactivity effect, with respect to its reference value, as a weighted sum of the complete collection of cell-wise data and/or modelling discrepancies. The current paper outlines the basic theory and gives certain practical applications of the proposed decomposition methodology.

1. INTRODUCTION

The accurate estimation of integral reactor physics parameters associated with detailed reactivity balance is essential for achieving high reliability in fuel design and nuclear power plant operation. From the safety assessment viewpoint, this concerns quantities such as core excess reactivity, shutdown pin worths and reactivity coefficients. Modern boiling water reactor (BWR) fuel assembly designs include complex localised features intended for maintaining a well-determined reactivity balance. For instance, part-length fuel rods (i.e., pins of reduced length, placed in the lower part of the assembly such that the pin is replaced by coolant at the top) serve several purposes, e.g. to increase the shutdown margin. In this context, it is important to show that one is able to accurately calculate the reactivity difference between a nominal BWR lattice and one in which, for example, one or more pins are replaced by water.

Since the operational margins required to avoid possible failures relate to several standard deviations, an improved knowledge about the accuracy of reactivity calculations will signify significant gains in performance. The benefit will not only be to eliminate overconservatism in the operational and safety limits themselves, but also, through additional validation of code capability for accurate prediction of power distributions, to establish an increased and more accurately known end-of-life burnup for the nuclear fuel, so as to eventually reduce uncertainties in transport, storage and disposal problems related to criticality, dose rates and radiotoxicity.

To meet the above goals, the Swiss Nuclear Utilities and the Paul Scherrer Institute have jointly set up the LWR-PROTEUS programme[1], a series of different experimental phases aimed at providing an up-to-date validation base for LWR fuel design and core analysis tools via accurate measurements of reactivity effects and reaction-rate distributions in modern LWR fuel.

In comparing calculated and measured reactivity effects, it is of importance to have a thorough understanding of how an integral difference between "real life" conditions and a calculational model results from space, processtype and energy-dependent effects in fuel pin-wise reaction rates. Analogously, in intercomparing different codes, one is interested in how certain specific numerical property differences between two different calculational models will propagate into phase-space integrated differences in corresponding calculated reactivity effects.

For this purpose, a reactivity effect decomposition approach has been developed that allows an optimized breakdown of the reactivity effect in terms of individual space, process-type and energy-dependent subcontributions. By definition, these subcontributions can be interpreted as importance weights quantifying the partial integrated reactivity effect uncertainty contributions of localised space and energy-dependent flux and cross section uncertainties. As such, this approach has turned out to be a very helpful tool in the detection of sources of integrated reactivity effect discrepancies between numerical results generated by different codes, as well as between numerical and measurement results.

2. DETAILED BREAKDOWN OF INTEGRAL REACTIVITY EFFECTS

The approach presented here aims at quantifying individual space, process-type and energy-dependent contributions to a total reactivity effect. At the basis of this approach is the application of the exact equation[2,3] for a reactivity change due to operator changes caused by a perturbation in material composition,

$$\Delta\rho = \frac{\langle\phi^*|-\mathbf{A}-\mathbf{L}+(1-\rho)\mathbf{F}|\Delta\phi\rangle}{\langle\phi^*|\mathbf{F}'\phi'\rangle} + \frac{\langle\phi^*|-\Delta\mathbf{A}+(1-\rho)\Delta\mathbf{F}|\phi'\rangle}{\langle\phi^*|\mathbf{F}'\phi'\rangle} \quad , \tag{1}$$

with ρ the (unperturbed) reactivity, ϕ' the perturbed space and energy-dependent flux and ϕ^* the adjoint flux. The symbols **A**, **L** and **F** denote the absorption, leakage and production operator, respectively, with **A'**, **L'** and **F'** denoting the perturbed operators (i.e. **F'**=**F** + Δ**F**, Δ**F** being the imposed change in **F**). The inner product $\langle\phi^*|\mathbf{F}'|\phi'\rangle$ is defined as

$$\langle\phi^*|\mathbf{F}'|\phi'\rangle = \int_{\mathrm{V}}\int_0^\infty\int_{4\pi}\phi^*(\underline{\mathrm{r}},\mathrm{E},\underline{\Omega})\mathbf{F}'(\underline{\mathrm{r}},\mathrm{E},\underline{\Omega})\phi'(\underline{\mathrm{r}},\mathrm{E},\underline{\Omega})\mathrm{d}\Omega\mathrm{d}\mathrm{E}\mathrm{d}\mathrm{V} \quad . \tag{2}$$

Since, in transport theory, the radial leakage operator $\mathbf{L} = \underline{\Omega}\cdot\underline{\nabla}$ is invariant under local material composition perturbations, $\Delta\mathbf{L} = 0$ by definition. Obviously, if ϕ^* is an exact solution of the adjoint equation

$(\mathbf{A}^* + \mathbf{L}^* - \lambda\mathbf{F}^*)\,\phi^* = 0$, the numerator in the second term would disappear. However, it is important to realize that, in numerical practice, also the iteratively obtained solution of the *adjoint* equation will generally *not* be exactly equal to the *exact* adjoint flux, but rather be a good approximation: $\tilde{\phi^*} = \phi^* + \tilde{\epsilon^*}$. Therefore, for preserving an unconditionally valid expression for the eigenvalue change due to a localised material composition change, we chose to keep the term $\langle\phi^*|\,(\mathbf{A} + \mathbf{L} - \lambda\mathbf{F})\,\Delta\phi\rangle$ present in the development. In this way, the adjoint flux is allowed to have imperfections. In fact, substitution by any arbitrary nonzero premultiplier (like, for example, the unity function) would preserve the exact validity of Eq.(1). According to this expression, it is possible to define space-wise contributions to the total reactivity effect, by writing the inner products in the numerator of Eq.(1) as sums of n subproducts, defined in the n different individual material volume regions (e.g. fuel pin cells) that together add up to the total system volume under consideration:

$$\langle\cdots|\cdot\cdot\rangle = \sum_{\mathrm{i}=1}^{\mathrm{n}}\langle\cdots|\cdot\cdot\rangle_{\mathrm{i}} \stackrel{\mathrm{def}}{=} \sum_{\mathrm{i}=1}^{\mathrm{n}}\int_{\mathrm{V_i}}\int_0^\infty\int_{4\pi}\cdots\cdots\,\mathrm{d}\Omega\mathrm{d}\mathrm{E}\mathrm{d}\mathrm{V} \tag{3}$$

Obviously, $\Delta\mathbf{A}$ and $\Delta\mathbf{F}$ will be 0 everywhere except in the perturbation position itself since the operators $\mathbf{A}$ and $\mathbf{F}$ are represented, in a mesh-wise sense, by diagonal matrices. In what follows, we will, for mathematical convenience, continue the formalism in terms of *eigenvalue* rather than reactivity changes. Realizing that $\rho = 1 - 1/\mathrm{k_{eff}} = 1 - \lambda$, with λ the eigenvalue, the simple relationship between the reactivity change and the eigenvalue change is $\Delta\rho = -\Delta\lambda$. Now, introducing a convenient separation between the perturbation location p and the rest of the system, we obtain

$$\Delta\lambda = \frac{\langle\phi^*|\Delta(\mathbf{A} - \lambda\mathbf{F})|\phi'\rangle_{\mathrm{p}} + \langle\phi^*|\mathbf{A} + \mathbf{L} - \lambda\mathbf{F}|\Delta\phi\rangle_{\mathrm{p}} + \sum_{\mathrm{i}\neq\mathrm{p}}\langle\phi^*|\mathbf{A} + \mathbf{L} - \lambda\mathbf{F}|\Delta\phi\rangle_{\mathrm{i}}}{\langle\phi^*|\mathbf{F}'\phi'\rangle} \tag{4}$$

Defining the *cell-wise eigenvalue change decomposition terms* $\Delta\lambda^{(\mathrm{i})}$ formally as

$$\Delta\lambda^{(\mathrm{i})} = \frac{\left[\langle\phi^*|\Delta(\mathbf{A} - \lambda\mathbf{F})|\phi'\rangle_{\mathrm{p}} + \langle\phi^*|\mathbf{A} + \mathbf{L} - \lambda\mathbf{F}|\Delta\phi\rangle_{\mathrm{p}}\right]\delta_{\mathrm{ip}} + \langle\phi^*|\mathbf{A} + \mathbf{L} - \lambda\mathbf{F}|\Delta\phi\rangle_{\mathrm{i}}}{\langle\phi^*|\mathbf{F}'\phi'\rangle}\ , \tag{5}$$

we can write $\Delta\lambda$ as a sum over cell-wise constituents $\Delta\lambda^{(\mathrm{i})}$: $\Delta\lambda = \sum_{\mathrm{i}=1}^{\mathrm{n}}\Delta\lambda^{(\mathrm{i})}$. The more accurately ϕ^* satisfies the adjoint equation, the smaller the *explicit* contributions from cells other than the perturbation cell(s) become, according to the definition of the $\Delta\lambda^{(\mathrm{i})}$ in Eq.(5). Implicitly of course, the influence of surrounding cells, through neutronic coupling, is represented in ϕ^*_{p}, through the denominator $\langle\phi^*|\mathbf{F}'\phi'\rangle$ and in the value of ${\phi_{\mathrm{p}}}'$. Thus, in case the adjoint equation would be satisfied *exactly*, $\Delta\lambda^{(\mathrm{i})} = 0$ for unperturbed cells i and $\Delta\lambda^{(\mathrm{p})} = \Delta\lambda$:

$$\lim_{\phi^*\to\phi^*_{\mathrm{exact}}}\Delta\lambda^{(\mathrm{i})} = \Delta\lambda\delta_{\mathrm{i,p}} \tag{6}$$

with $\delta_{\mathrm{i,p}}$ being the Kronecker delta, equalling 1 in the case i=p and 0 otherwise. Obviously, energy- and isotopewise subdecomposition can be applied for the $\Delta\lambda^{(\mathrm{i})}$, effecting the extended decomposition of total inner products, analogous to Eq.(3), as

$$\langle\cdots|\cdot\cdot\rangle = \sum_{\mathrm{i}=1}^{\mathrm{n}}\sum_{\mathrm{g}=1}^{\mathrm{G}}\sum_{\mathrm{q}=1}^{\mathrm{Q}}\langle\cdots|\cdot\cdot\rangle_{\mathrm{igq}} \stackrel{\mathrm{def}}{=} \sum_{\mathrm{i}=1}^{\mathrm{n}}\sum_{\mathrm{g}=1}^{\mathrm{G}}\sum_{\mathrm{q}=1}^{\mathrm{Q}}\int_{\mathrm{V_i}}\int_{\mathrm{E_{g-1}}}^{\mathrm{E_g}}\int_{4\pi}\cdots\cdots\,\mathrm{d}\Omega\mathrm{d}\mathrm{E}\mathrm{d}\mathrm{V} \tag{7}$$

with g and q being labels for energy group and nuclide type, respectively. The total number of material regions, applied energy groups and modelled nuclide-types are denoted by n, G and Q, respectively. In addition to this extended decomposition, one can distinguish between *process-associated* reaction rates. For example, each partial fissile nuclide-q-wise contribution to the g-group component of the absorption operator can be decomposed into its capture and its fission parts:

$$\Sigma^{\mathrm{A}}_{\mathrm{igq}} = \Sigma^{\mathrm{C}}_{\mathrm{igq}} + \frac{1}{\nu_{\mathrm{gq}}}\Sigma^{\nu\mathrm{F}}_{\mathrm{igq}} \tag{8}$$

such that the decomposition can be extended in terms of space, energy, isotopewise contributions to the capture (C), leakage (L) and fission (F) differentiated contributions to the total reactivity effect:

$$\Delta\lambda = \sum_{\mathrm{i}=1}^{\mathrm{n}}\sum_{\mathrm{g}=1}^{\mathrm{G}}\sum_{\mathrm{q}=1}^{\mathrm{Q}}\left[\Delta\lambda^{(\mathrm{C})}_{\mathrm{igq}} + \Delta\lambda^{(\mathrm{L})}_{\mathrm{igq}} + \Delta\lambda^{(\mathrm{F})}_{\mathrm{igq}}\right] . \tag{9}$$

With the choice of the adjoint flux ϕ^* (or a sufficiently good approximation for ϕ^*) for the premultiplying function in Eq.(5), the $\lambda^{(\mathrm{m})}_{\mathrm{igq}}$ (with m indicating the process type: capture, leakage or fission) have the physical meaning of first-order sensitivity coefficients. In terms of the formalism applied here, discrepancies in cross-sections and neutron flux are *coupled* in the sense that a discrepancies in flux have to be associated with (i.e. follow from) discrepancies, to be identified, in the operators. As such , in case $\mathrm{i} \neq \mathrm{p}$, the contributions $\Delta\lambda^{(\mathrm{m})}_{\mathrm{igq}}$ serve as importance weight coefficients that quantify the sign and magnitude with which individual operator discrepancies in cell i (other than the perturbed cell p) contribute to the total integrated discrepancy in the prespecified reactivity effect. For arguing this mathematically, we consider a cell-wise (i), energy-group (g) dependent, process-type (m), isotope-q-characteristic cross-section $\Sigma^{(\mathrm{igmq})}$. The effect of an uncertainty in this cross section can be written as

$$\Sigma^{(\mathrm{igmq})} \rightarrow \Sigma^{(\mathrm{igmq})} + \delta\Sigma^{(\mathrm{igmq})} \tag{10}$$

Obviously, this particular uncertainty will, through the neutron balance equation, result in an associated uncertainty $\delta^{(\mathrm{igmq})}\phi$ in the a priori perturbed flux solution such that $\phi' \rightarrow \phi' + \delta^{(\mathrm{igmq})}\phi' = \phi + \Delta\phi + \delta^{(\mathrm{igmq})}\phi'$. Thus, the isolated igmq-contribution of this adjustment on the calculated reactivity effect can be expressed in first-order approximation as

$$\delta^{(\mathrm{igmq})}\left[\Delta\lambda\right] = \delta^{(\mathrm{igmq})}\left[\lambda'\right] - \delta^{(\mathrm{igmq})}\left[\lambda\right] \simeq \frac{\langle\phi^*|\Delta\mathbf{A} - \lambda\Delta\mathbf{F}|\delta^{(\mathrm{igmq})}\phi'\rangle_{\mathrm{p}}}{\langle\phi^*|\mathbf{F}'\phi'\rangle}\,\delta_{\mathrm{i,p}}$$

$$+ \frac{\langle\phi^*|\delta\Sigma^{(\mathrm{igmq})}|\Delta\phi\rangle_{(\mathrm{igmq})}}{\langle\phi^*|\mathbf{F}'\phi'\rangle} + \frac{\langle\phi^*|\mathbf{A} + \mathbf{L} - \lambda\mathbf{F}|\delta^{(\mathrm{igmq})}\phi'\rangle}{\langle\phi^*|\mathbf{F}'\phi'\rangle} \quad , \tag{11}$$

in the development of which the first term vanishes for all cells other than the perturbation cell itself ($\mathrm{i} \neq \mathrm{p}$). With ϕ^* being sufficiently close to the exact adjoint flux, the unquantifiable third term in Eq.(11) reduces to 0 in any case. Defining the cross-section uncertainty in fractional form, $\epsilon[\Sigma^{(\mathrm{igmq})}] = \delta\Sigma^{(\mathrm{igmq})}/\Sigma^{(\mathrm{igmq})}$, we acquire the following result for $\mathrm{i} \neq \mathrm{p}$:

$$\delta^{(\mathrm{igmq})}\left[\Delta\lambda\right] \simeq \frac{\langle\phi^*|\Sigma^{(\mathrm{igmq})}|\phi\rangle_{(\mathrm{igmq})}}{\langle\phi^*|\mathbf{F}'\phi'\rangle}\,\epsilon[\Sigma^{(\mathrm{igmq})}] \stackrel{\mathrm{def}}{=} \Delta\lambda^{(\mathrm{m})}_{\mathrm{igq}}\,\epsilon[\Sigma^{(\mathrm{igmq})}] \ , \tag{12}$$

which indicates that the $\Delta\lambda_{igq}^{(m)}$ are in fact *uncertainty propagation weight coefficients* for the total integrated reactivity effect. For $i = p$, a similar exact expression would have resulted when using the perturbed rather than the unperturbed adjoint flux. The property expressed in Eq.(12) means that, when viewing a map of space-wise reactivity effect contributions (optionally further decomposed with respect to process-type, energy-group and isotope-type) whose calculation was based on the choice of the adjoint flux (or an adequate approximation thereof) as a premultiplier, one is simultaneously viewing a sensitivity map. In this map, the values in the cells other than the perturbation cell itself indicate the importance of the potential contribution to the integrated reactivity effect discrepancy in case of occurring uncertainties. Practical examples of these and a discussion on how these can be used in the understanding and quantification of reactivity discrepancies in practice, can be found in the following section.

3. APPLICATION IN LWR-PROTEUS

The LWR-PROTEUS[1,4,5,6] experiments have been set up jointly by the Swiss Nuclear Utilities and PSI for providing an up-to-date validation base for LWR fuel design and core analysis tools (such as CASMO-4, BOXER and HELIOS) via accurate measurements of reaction rate distributions and reactivity effects in modern LWR fuel. The decomposition methodology could be applied very effectively to the analysis of *fuel-rod removal reactivity effect*[6] measurements in LWR-PROTEUS Phase I, the test zone consisting of a 3x3 arrangement of SVEA-96+ BWR assemblies. Each individual fuel pin removal experiment consists of measuring the reactivity effect of replacing the specific fuel pin in the central test assembly by water in an initially critical configuration. The reactivity worth of a given fuel pin is determined by its material composition (i.e. enrichment level, possible gadolinium content, etc.) and by the coupled neutron field and material properties of its surroundings. As indicated in Fig.1, these surroundings can consist of simply other fuel pins (UO_2 with or without Gd), or of a combination of fuel pins and water regions.

Due to the coupling of the material density field and the flux distribution, the effect of the removal of a fuel pin on the spatial flux distribution is not confined to merely the pin position itself. Because of this, the change in reactivity due to the pin removal originates, in a spatial sense, from a perturbation in the neutronics bookkeeping of basically the whole system, with the most important contributions originating from the pin-removal position itself and its immediate surroundings. This implies that a discrepancy in the reactivity worth of any specific fuel pin is a composite of several different propagated discrepancies with varying signs originating, in principle, from the entire modelled system.

Due the fact that neither CASMO-4 nor BOXER offer the capability of calculating the space, energy and angle-dependent adjoint flux, it was decided to apply TWODANT for this purpose, by modelling the configurations of interest in a TWODANT input file as well and selecting the option for calculation of the fundamental multi-group adjoint mode. This is a typical case of the approach where, instead of using the exact adjoint flux distribution (as characteristic for the CASMO-4 and BOXER solution, respectively), an approximated form, in this case generated by another code, is applied due to the unavailability of the exact adjoint for the case of interest. As pointed out before in section 2, however, this is not a problem since the choice of a premultiplying function that is close enough to the postulated exact solution will, on top of preserving the exact validity of the decomposition, still enable the valuable pursuit of discrepancy source detection analysis.

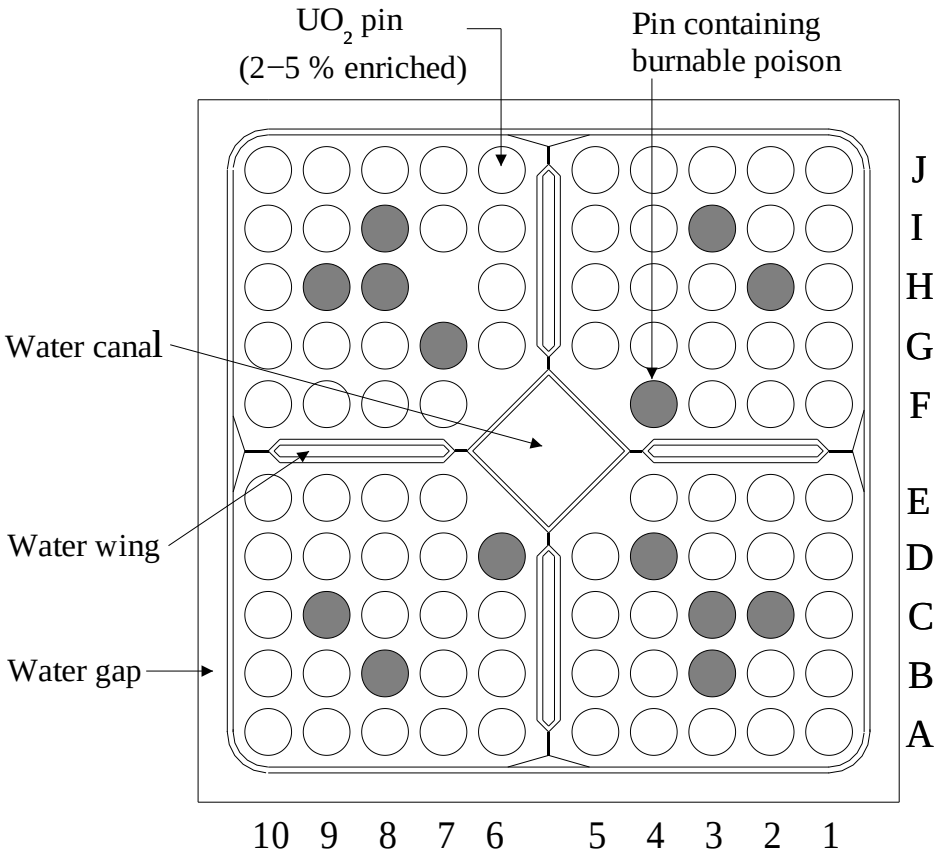

Figure 1 SVEA-96+ assembly geometry (as in LWR-PROTEUS Core 1A), in which the removal of UO_2 pin H7 is illustrated.

In the actual LWR-PROTEUS situation, of a square fuel assembly surrounded by 8 identical square assemblies, infinite lattice conditions are a good approximation for the internal flux distributions in the central assembly. In the present context, this is adequate justification for applying *reflective boundary conditions* at the assembly edges, leading to a practically flat adjoint flux distribution. Because of this, the decompositions would hardly have been different numerically if one would have applied the unit function as a premultiplier in the definition of the $\Delta\lambda_{\mathrm{i}}$'s. This has been verified numerically. Realizing this, the total sum of calculated leakage-associated reactivity effect contributions, $\sum_{\mathrm{i}} \Delta\lambda_{\mathrm{i}}^{(\mathrm{L})}$, can be argued to be approximately proportional to the physical total radial leakage which, under the infinite lattice property imposed by the reflective boundary conditions, equals 0 (since no radial leakage can occur from a two-dimensional infinite system). Therefore, in this particular case, the sum $\sum_{\mathrm{i}} \left[\Delta\lambda_{\mathrm{i}}^{(\mathrm{C})} + \Delta\lambda_{\mathrm{i}}^{(\mathrm{F})}\right]$, with the $\Delta\lambda_{\mathrm{i}}^{(\mathrm{L})}$'s omitted, will be very close to $\Delta\lambda$.

For comparing calculational results with reality, in which a net neutron leakage occurs from the central assembly (constituting a departure from the currently imposed infinite lattice conditions), one has of course to correct the $\Delta\lambda_{\mathrm{i}}^{(\mathrm{m})}$'s for each process-m type such that the total $\Delta\lambda$ can be compared indeed with a measured result. Also here, the decomposition method is proving to be very valuable, enabling a

detailed correction of the reactivity effect integral by individual corrections of the cell-wise subintegrals. This development will be reported separately.

An example of a spatial decomposition map is shown in Fig.2, illustrating the thermal and fast capture (C) and fission (F)-bundled reactivity effect decompositions $\Delta\lambda_i^{(C)}$ and $\Delta\lambda_i^{(F)}$ obtained with CASMO-4 for the case in which UO_2-rod H7 is removed from LWR-PROTEUS configuration 1A.

As is reflected in Fig.2, at the position H7 itself the change from fuel to pure moderator gives rise to a local negative contribution to the total effect, as the negative effect of local fission loss has a higher weight than the positive reactivity effect of the vanished capture at that position. Because of the fact that, due to the pin removal, an 'island' of moderating material emerges at position H7, the thermal flux level is increased significantly at H7 itself, as well as in its direct surroundings. Due to this, the thermal fission rate in directly surrounding UO_2-pins is raised, constituting positive contributions that thus countercompensate the total negative reactivity effect. Analogously, the thermal capture rate in neighbouring Gd-pins is raised noticeably, such that these give significant negative contributions of the same sign as the local negative contribution of the position where the UO_2-pin was removed. The significant magnitude of contributions by clusters of Gd-containing pins also implies that possible discrepancies or nuclear data inconsistencies in the modelling of the Gd-pins can be expected to propagate noticeably into the value of the calculated reactivity worth of a nearby UO_2-pin. Indeed, from the post-comparison[6] of measured pin worths for configurations 1A and 1B, it has turned out that the presence of a Gd-cluster close to a UO_2-rod increases the likelihood for the occurrence of a noticeable departure from good agreement.

In the thermal and fast C-subdecompositions, a positive value in a cell represents a positive partial reactivity effect associated with a *decrease* in capture rate. In the thermal and fast F-subdecompositions, a positive value in a cell represents a positive partial reactivity effect associated with an *increase* in fission rate. Triggered by the observation of noticeable differences[6] in calculated reactivity effects between CASMO-4 and BOXER, a detailed quest for the origin of these differences was initiated. An intercomparison of the decomposition distributions has pointed out that the difference in integrated reactivity effect between BOXER and CASMO-4 originates mainly from how the shape of the *thermal* flux elevation is reconstructed differently by BOXER and CASMO-4. This basic numerical discrepancy between BOXER and CASMO-4 could, via a visualization of how individual reactivity change contributions are affected (both in the C- and in the F-range), be shown to be the *principal source* of the integrated discrepancies in calculated pin removal worths between BOXER and CASMO-4, not only for pin H7, but in general for every pin, as became clear from the application of the decomposition analysis to other pins. Since the upward peak in thermal flux around the pin removal position is a bit broader according to the BOXER results when compared to the CASMO-4 results, the relative thermal flux increase at the removal position itself is somewhat lower predicted by BOXER compared to CASMO-4, whereas the wings of the peak that cover the positions surrounding the pin removal location are somewhat higher than compared to CASMO-4. This numerical difference effect is illustrated in Fig.3.

Due to the effect described above, the (countercompensating) reactivity effect contributions of surrounding UO_2-pins positions will be somewhat higher when calculated by BOXER compared to values calculated by CASMO-4. In case of the removal of a rather centralized UO_2-pin, surrounded mainly by other UO_2-pins, this phenomenon can be expected, and has indeed been observed, to give rise to rather severe underpredictions[6] of the total reactivity change as calculated by BOXER, depending on the importance of the reactivity effect contributions of the directly surrounding positions. Important examples are the BOXER results[6] obtained for the pins C7, D8 and E8. The spatial reactivity effect contributions around these low worth positions fluctuate strongly, featuring high positive and negative values that,

CASMO-4 C-contributions to the total reactivity change, in percent of the total effect

	10	9	8	7	6		5	4	3	2	1
J	0.36	0.13	-0.31	-0.96	-0.82	-0.14	-0.26	-0.06	0.03	0.07	0.08
	0.31	0.29	0.23	0.17	0.17	0.01	0.16	0.12	0.08	0.06	0.03
I	0.26	-0.01	-12.45	-4.20	-2.36	-0.24	-0.48	-0.12	0.02	0.04	0.05
	0.29	0.25	-0.24	-0.56	-0.24	0.01	0.14	0.11	0.12	0.05	0.03
H	0.21	-1.07	-26.73	9.89	-4.64	-0.34	-0.62	-0.15	-0.02	0.20	0.04
	0.28	0.26	-0.75	29.54	-0.65	0.01	0.12	0.10	0.07	0.07	0.03
G	0.16	-0.19	-1.17	-30.56	-1.96	-0.24	-0.46	-0.13	-0.02	0.01	0.03
	0.26	0.21	-0.21	-0.84	-0.26	0.01	0.12	0.10	0.06	0.04	0.02
F	0.16	-0.05	-0.30	-0.43	-0.26	-0.14	-0.12	-0.63	0.00	0.01	0.01
	0.23	0.22	0.16	0.11	0.01	0.00	0.01	0.13	0.05	0.02	0.01
	0.05	0.01	-0.02	-0.04	-0.06	-0.03	-0.03	0.00	0.00	0.00	0.00
	0.01	0.01	0.01	0.01	0.00	0.00	0.00	0.00	0.00	0.00	0.00
E	0.18	0.08	0.01	-0.04	-0.03	-0.01	-0.01	0.01	0.01	0.00	0.00
	0.17	0.17	0.16	0.14	0.01	0.00	0.00	0.05	0.03	0.01	-0.01
D	0.15	0.09	0.05	0.03	0.19	0.00	0.02	0.15	0.01	0.00	-0.01
	0.13	0.12	0.11	0.11	0.14	0.00	0.06	0.05	0.01	-0.01	-0.02
C	0.13	0.69	0.04	0.04	0.04	0.01	0.02	0.01	0.01	-0.15	-0.04
	0.09	0.13	0.08	0.07	0.06	0.00	0.03	0.01	-0.01	-0.03	-0.03
B	0.11	0.07	0.42	0.04	0.03	0.01	0.02	0.00	-0.12	-0.03	-0.05
	0.06	0.06	0.08	0.04	0.03	0.00	0.01	-0.01	-0.03	-0.03	-0.04
A	0.11	0.08	0.06	0.05	0.04	0.01	0.01	-0.01	-0.04	-0.04	-0.07
	0.04	0.04	0.03	0.02	0.01	0.00	-0.01	-0.02	-0.03	-0.04	-0.04

thermal
fast

CASMO-4 F-contributions to the total reactivity change, in percent of the total effect

	10	9	8	7	6		5	4	3	2	1
J	-1.02	-0.42	1.14	3.55	2.83	0.00	0.91	0.21	-0.09	-0.18	-0.18
	-0.13	-0.15	-0.12	-0.05	-0.04	0.00	-0.05	-0.04	-0.02	-0.01	0.00
I	-0.90	0.03	0.27	17.00	9.46	0.00	1.93	0.48	-0.01	-0.14	-0.18
	-0.16	-0.17	-0.09	0.11	0.06	0.00	-0.04	-0.04	-0.02	-0.01	0.00
H	-0.76	0.03	0.57	-94.83	18.78	0.00	2.49	0.63	0.09	-0.01	-0.13
	-0.17	-0.13	-0.09	-26.55	0.21	0.00	-0.03	-0.03	-0.02	-0.01	0.00
G	-0.57	0.76	4.67	0.64	7.53	0.00	1.61	0.54	0.07	-0.05	-0.09
	-0.15	-0.15	-0.06	-0.05	0.04	0.00	-0.02	-0.04	-0.02	-0.01	0.01
F	-0.58	0.18	1.20	1.63	0.00	0.00	0.00	0.00	-0.02	-0.06	-0.06
	-0.12	-0.14	-0.10	-0.07	0.00	0.00	0.00	-0.03	-0.01	0.00	0.02
	0.00	0.00	0.00	0.00	0.00	0.00	0.00	0.00	0.00	0.00	0.00
	0.00	0.00	0.00	0.00	0.00	0.00	0.00	0.00	0.00	0.00	0.00
E	-0.61	-0.36	-0.04	0.14	0.00	0.00	0.00	-0.02	-0.05	-0.03	0.01
	-0.09	-0.10	-0.09	-0.06	0.00	0.00	0.00	-0.02	0.00	0.02	0.02
D	-0.55	-0.34	-0.19	-0.10	-0.02	0.00	-0.07	-0.01	-0.03	0.01	0.07
	-0.07	-0.07	-0.07	-0.06	-0.04	0.00	-0.02	0.00	0.01	0.03	0.03
C	-0.45	-0.03	-0.18	-0.15	-0.14	0.00	-0.09	-0.04	0.00	0.00	0.12
	-0.05	-0.04	-0.04	-0.03	-0.03	0.00	0.00	0.01	0.02	0.02	0.04
B	-0.37	-0.26	-0.02	-0.15	-0.13	0.00	-0.06	-0.01	0.00	0.11	0.18
	-0.02	-0.03	-0.02	-0.01	-0.01	0.00	0.01	0.02	0.02	0.04	0.04
A	-0.31	-0.27	-0.21	-0.15	-0.10	0.00	-0.01	0.04	0.10	0.18	0.21
	-0.01	-0.01	-0.01	0.00	0.01	0.00	0.02	0.03	0.04	0.04	0.04

thermal
fast

Fig.2. Thermal and fast components of the subdecompositions $\Delta\lambda_i^{(C)}$ (top picture) and $\Delta\lambda_i^{(F)}$ (bottom picture), normalized to a total reactivity effect of -100 %, obtained by CASMO for the removal of UO_2-pin H7 in LWR-PROTEUS configuration 1A.

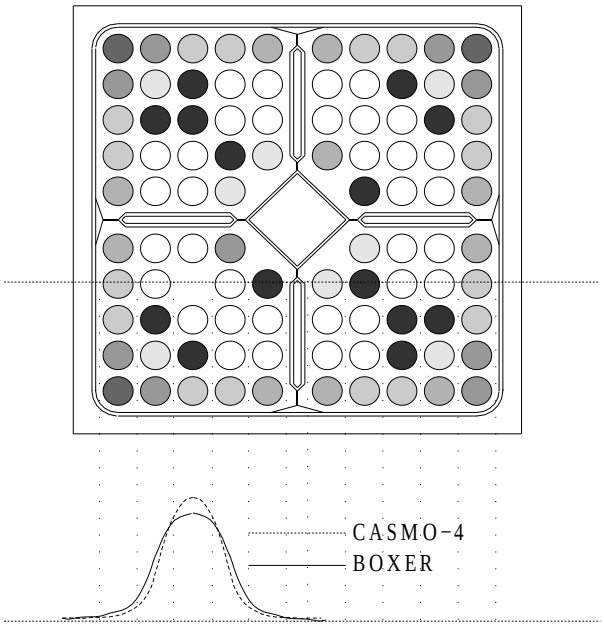

Fig.3. Numerical difference between BOXER and CASMO in the calculation of the thermal flux elevation due to the removal of UO_2-rod D8 in LWR-PROTEUS configuration 1A.

	10	9	8	7	6		5	4	3	2	1
J	-0.37	-0.42	-0.49	-0.42	-0.37	0.05	-0.25	-0.13	0.01	0.06	0.09
	-0.30	-0.30	-0.40	-0.30	-0.30	0.00	-0.20	-0.20	-0.20	-0.20	-0.10
I	-0.33	-0.30	1.19	-0.26	-0.32	0.04	-0.33	-0.17	0.49	-0.01	-0.01
	-0.40	-0.20	1.10	-0.20	-0.30	0.00	-0.30	-0.10	0.60	-0.10	-0.20
H	0.02	0.20	-0.05	0.01	-0.03	0.02	-0.24	-0.20	-0.16	0.62	-0.13
	-0.10	0.50	0.30	0.00	-0.20	0.00	-0.20	-0.10	-0.10	0.60	-0.20
G	0.83	1.32	1.51	-2.89	0.72	-0.01	0.06	-0.20	-0.27	-0.29	-0.28
	0.30	0.60	0.60	-0.80	0.20	0.00	0.80	-0.10	-0.10	-0.10	-0.20
F	2.42	4.58	5.79	4.63	-0.38	-0.10	-0.02	1.12	-0.40	-0.48	-0.50
	1.20	2.50	2.90	1.70	-0.10	0.00	0.10	1.00	-0.20	-0.30	-0.20
	-0.44	-0.70	-1.00	-0.76	-0.49	-0.13	-0.04	0.03	0.05	0.06	0.08
	-0.20	-0.40	-0.50	-0.20	-0.10	0.00	0.00	0.00	0.00	0.00	0.00
E	6.54	19.71	39.52	15.36	-1.03	-0.24	-0.09	-0.08	-0.45	-0.59	-0.62
	3.80	12.10	22.80	-29.10	-0.30	0.00	0.00	-0.10	-0.20	-0.30	-0.30
D	8.36	35.30	-249.25	35.38	-24.75	-0.12	0.73	0.88	-0.37	-0.55	-0.74
	5.60	15.90	-134.30	17.00	-13.30	0.00	0.30	0.70	-0.10	-0.20	-0.30
C	3.84	-44.10	31.91	15.84	5.07	-0.09	0.43	-0.17	1.44	2.16	-0.86
	2.40	-29.50	15.90	8.30	3.20	0.00	0.20	0.00	0.80	1.00	-0.30
B	1.11	2.52	-18.14	4.60	2.14	-0.02	-0.11	-0.48	2.31	-0.77	-0.87
	0.50	1.30	-12.40	2.20	1.40	0.00	-0.10	-0.20	1.20	-0.20	-0.40
A	0.07	0.33	0.37	0.66	0.26	0.08	-0.56	-0.85	-0.97	-0.89	-0.83
	-0.20	0.00	0.10	0.40	0.10	0.10	-0.30	-0.50	-0.40	-0.40	-0.30

1A
1B

Fig.4 Group-collapsed decomposition maps, normalized to -100%, obtained, using CASMO-4, for the removal of UO_2 pin D8 in LWR-PROTEUS configurations 1A and 1B.

added together, cancel largely and eventually produce an actually rather small reactivity change. This behaviour is illustrated most clearly in the 1A-part of Fig.4, displaying the CASMO-4 reactivity effect decomposition for the case of the removal of UO_2-pin D8, as occurring in configuration 1A (top values in cells) compared with the values for configuration 1B (bottom values). It is in such a situation that the basic numerical discrepancy between BOXER and CASMO-4, illustrated in Fig.3, is amplified significantly through the strongly fluctuating decomposition distribution. The decomposition distribution acts as a discrepancy propagation sensitivity/weight matrix for the eigenvalue change, leading –in the case of pin D8– to the strongly amplified downward deviation in the case of BOXER compared to CASMO-4. The reason why the total reactivity change is relatively small for pin D8 in configuration 1A is that it is surrounded by a maximum number of UO_2-neighbours. The countercompensating contributions of these neighbours are overpredicted by BOXER (compared to CASMO-4), thus leading to a large *under*prediction of the net reactivity change.

It is interesting to note that, in the case of configuration 1B, much less strongly fluctuating spatial contributions are found for the same pin position because of the different local material composition distribution. For the case of removing pin D8 this is illustrated in Fig.4, in which a comparison of the D8-decomposition maps is presented for configurations 1A and 1B. As a consequence, the differences between BOXER and CASMO-4 (and also the underpredictions[6] by BOXER with respect to measurement results) for the positions C7, D8, E8 are much smaller in configuration 1B than in configuration 1A. The comparisons between calculated and measured results for 1A and 1B are presented and discussed extensively in Ref.6.

CONCLUSIONS

A convenient analytical approach for reactivity effect uncertainty assessment in lattice physics, referred to as the decomposition methodology, has been proposed. This method enables a quantification of the relative importance of different space, process-type and energy-dependent uncertainties that determine the integral uncertainty in a total reactivity effect associated with a prespecified material composition change. In the LWR-PROTEUS context of establishing an improved understanding of differences among pin removal reactivity effects as predicted by different codes, as well as between the predictions and experiments, this methodology has proved to be a very useful tool. The values of the individual contributions, defined in accordance with the presented decomposition equations, have the physical/mathematical meaning of elements of an uncertainty propagation importance weight matrix, providing the interface between the space, process-type and energy-group-characteristic data and/or modelling discrepancies on the one hand, and the integrated discrepancies in calculated reactivity effects that they give rise to, on the other.

A valuable application of the decomposition methodology is in helping to detect the source(s) of observed reactivity effect discrepancies. In the LWR-PROTEUS Phase I post-analysis of fuel pin removal reactivity effects, the decomposition methodology has proved to be very helpful in disclosing, in a space, process-type and energywise picture, from which spatial region, process-type and neutron energy range the most important contributions to an observed intercalculational reactivity (change) discrepancy originate. The application of the decomposition approach has provided an in-depth understanding, as well as the desired quantitative explanation, of observed extrema in comparisons between calculated and measured pin removal worths in the different experimental configurations investigated.

ACKNOWLEDGEMENTS

The LWR-PROTEUS programme is being conducted jointly by PSI and the Swiss Nuclear Utilities (UAK), with specific contributions from Elektrizitätsgesellschaft Laufenburg (EGL) and Aare-Tessin AG für Elektrizität (ATEL). We are particularly grateful to H. Achermann and T. Williams (EGL), H. Fuchs (ATEL), G. Meier (KKG), R. Stratton (NOK), D. Furtado (KKM), W. Kröger and R. Brogli (PSI) for their strong support of the experiments. Further, we wish to acknowledge P. Grimm and A. Meister for their useful contributions to discussions on the topic presented in this manuscript, as well as M. Murphy, A. Lüthi, R. Seiler, P. Bourquin, M. Berweger and R. Winter for their impeccable experimental work during PROTEUS Phase I.

REFERENCES

1) T. Williams, R. Chawla, P. Grimm, O. Joneja, R. Seiler, A. Ziver, "New Experiments at a Zero-Power Facility Using Power Reactor Fuel", *Proceedings of the International Conference on the Physics of Nuclear Science and Technology*, pp. 720-727, Long Island, USA (1998).

2) K.O. Ott, R.J. Neuhold,"*Introductory Nuclear Reactor Dynamics*", American Nuclear Society, La Grange Park, Illinois, USA (1985).

3) R. van Geemert, J.E. Hoogenboom, "Development of Parallellized Higher-Order Generalized Depletion Perturbation Theory for Application in Equilibrium Cycle Optimization", *Annals of Nuclear Energy*, Vol. **28**, 1377-1411 (2001).

4) O. Joneja, M. Plaschy, F. Jatuff, A. Lüthi, M. Murphy, R. Seiler, R. Chawla, 2001. "Validation of an MCNP4B Whole-Reactor Model for LWR-PROTEUS using ENDF/B-V, ENDF/B-VI and JEF-2.2 Cross-Section Libraries", Annals of Nuclear Energy, Vol. **28**, No. 7, pp. 701-713 (2001).

5) F. Jatuff, P. Grimm, O.P. Joneja, M. Murphy, A. Lüthi, R. Seiler, R. Brogli, R. Jacot-Guillarmod, T. Williams, S. Helmersson, and R. Chawla, "LWR-PROTEUS Verification of Reaction Rate Distributions in Modern 10x10 BWR Fuel", *Nuclear Science and Engineering* Vol. **139**, 262-272 (2001).

6) A. Meister *et al.*, "Experimental Investigation of Pin Removal Reactivity Worths for a Westinghouse SVEA-96+ Assembly in the PROTEUS Research Reactor", *proceedings of the International Conference on the New Frontiers of Nuclear Technology: Reactor Physics, Safety and High-Performance Computing (PHYSOR 2002)*, Seoul, Korea (2002).